

## Frequency Analysis of Magnetic Journal Bearing Instability for MMR Condition

Dokyuu Kim<sup>a</sup>, SeungJoon Baik<sup>b</sup>, Jeong Ik Lee<sup>a\*</sup>

<sup>a</sup>Department of Nuclear and Quantum Engineering, KAIST, Daejeon, South Korea

<sup>b</sup>Korea Atomic Energy Research Institute, Daejeon, South Korea

Corresponding author : [jeongiklee@kaist.ac.kr](mailto:jeongiklee@kaist.ac.kr)

### 1. Introduction

The attention on the distributed power generation with nuclear energy is increasing due to the electricity grid decentralization and demand for mobile power generation without emission of CO<sub>2</sub>. A concept of fully modularized fast reactor with a supercritical CO<sub>2</sub> (S-CO<sub>2</sub>) cooled direct Brayton cycle, namely Micro Modular Reactor (MMR), for 10MWe power output is developed for the distributed power generation based on the nuclear energy. Furthermore, MMR is being investigated for the potential application for marine propulsion to substitute a diesel engine due to newly released International Maritime Organization (IMO) regulation [1].

In the proposed MMR, an appropriate bearing technology for turbomachinery is required. First, the MMR turbomachinery should be designed to be hermetic type without lubrication fluid because lubrication fluid forces to add oil supply and sealing sub-system that complicates the system [2,3]. However, there are two types of hermetic type bearing: (1) gas bearing and (2) magnetic bearing. Gas bearing does not have enough load to support MMR turbomachinery condition. Therefore, magnetic type is a proper choice as supported by the previous research [4] and Fig. 1.

TM Feature	Power (MWe)					
	0.3	1.0	3.0	10	30	100
Bearings	Gas Foil		Hydrodynamic oil			
	Magnetic			Hydrostatic		

Fig. 1. Bearing options for S-CO<sub>2</sub> Brayton Cycles for various power scales [4]

However, an instability issue with magnetic bearing levitation was repeatedly mentioned under high speed operation and S-CO<sub>2</sub> conditions. With this instability, the shaft eccentricity can grow until the clearance disappears leading to rotor and stator contact. Shaft orbit regarding this issue is shown in Fig. 2. On the other hand, much higher speed operating in air condition does not have the same issue as shown in Fig. 3.

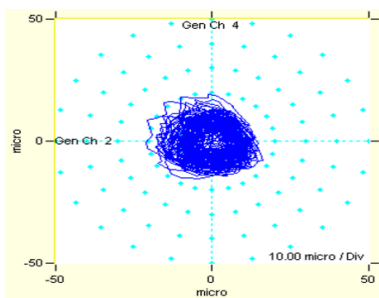


Fig. 2. Shaft center orbit at 14,000rpm, 43°C, 78 bar under S-CO<sub>2</sub> condition

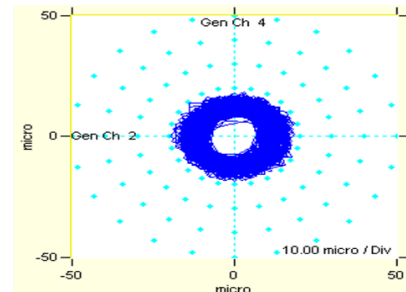


Fig. 3. Shaft center orbit at 30,000rpm under air condition

In this paper, the modeled S-CO<sub>2</sub> lubrication pressure distribution in the magnetic journal bearing geometry with uniform circular motion is analyzed with its physical properties. To explain and verify the results, the experimental results with shaft position is substituted into the model for comparison. Also, the results are analyzed with Fast Fourier Transform (FFT) method. The lubrication instability is discussed in view of the frequency analysis.

### 2. Methods and Results

#### 2.1 Lubrication analysis for flow induced force on shaft

Active-control magnetic bearing (AMB) levitates the rotating shafts with electromagnets to apply magnetic force. The force from an electromagnet is expressed as in eq. (1). The AMB's 8 electromagnets are located as shown in Fig. 4. The empty spaces in Fig. 4 is filled with the working fluid. The spaces potentially can generate vortices and it can destabilize the shaft.

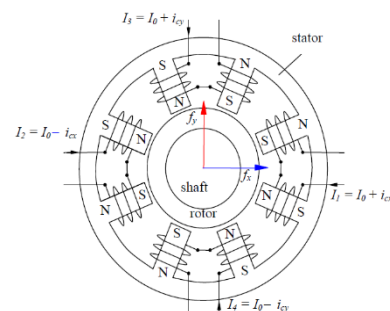


Fig. 4. Electromagnets in the magnetic bearing [5]

$$f = \frac{B^2 A_g}{2\mu_0} = \frac{\mu^2 N^2 I^2 A_g}{2\mu_0 l_g^2} \quad (1), [5]$$

The fluid force is caused by pressure distribution around the shaft. In this case, Reynolds equation is an appropriate governing equation to obtain this distribution. It can be given by substituting the velocity profile from

Navier-Stokes equation to the continuity equation for thin film [6]. The geometry for this equation is described in Fig. 5. In this research, the axial direction is assumed to be negligible because the axial velocity is relatively smaller than the  $u$ . Therefore, the governing equation can be simplified as in equation (2) with turbulence model which is described in Table I [7]. Before solving this equation, the transient term in right hand side (RHS) is handled by assuming the uniform circular motion. This is numerically solved by finite difference method (FDM) as shown in Fig. 5.

$$\frac{\partial}{\partial X} \left( \frac{\rho h^3}{k_x \mu} \frac{\partial p}{\partial X} \right) = \frac{1}{2} \frac{\partial(\rho h u)}{\partial X} + \frac{\partial(\rho h)}{\partial t} \quad (2)$$

( $t$  : time,  $u$  : circumferential velocity,  $\rho$  : density,  $\mu$  : viscosity.)  
( $k_x = 12 + K_x Re^{n_x}$ ,  $Re$  : Reynolds number)

Table I. Coefficient in Ng-Pan model

Reynolds number, $Re$	$K_x$	$n_x$
$50,000 < Re$	0.0388	0.8
$5000 < Re < 50000$	0.0250	0.84
$Re < 5000$	0.0039	1.06

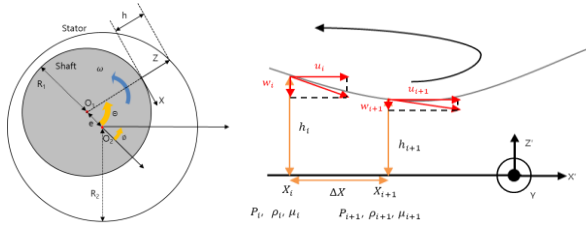


Fig. 5. Coordinate description of Reynolds equation with geometry of the unbalanced shaft and the stator

This analysis range is summarized in Table II. The modeling results are shown with the fluid force for various thermal properties as Fig. 6 and 7.

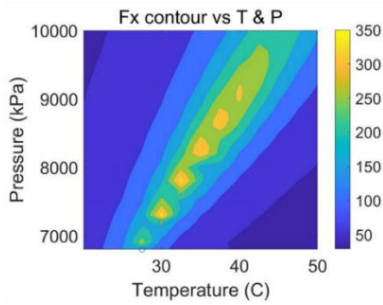


Fig. 6.  $F_x$  contour, 30000RPM,  $\epsilon=0.07$  ( $\epsilon$  : eccentricity ratio)

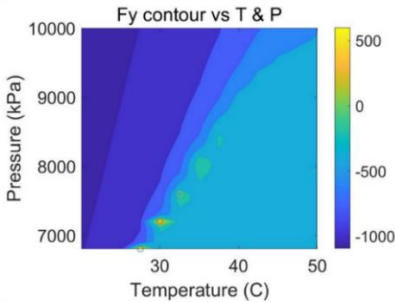


Fig. 7.  $F_y$  contour, 30000RPM,  $\epsilon=0.07$

Table II. Operation condition range of the model

Supply temperature	10 ~ 50 °C
Supply pressure	50 ~ 100bar
Rotational speed	30000 RPM
Eccentricity ratio, $\epsilon = e/(R_2 - R_1)$	0.07

Based on equation (2), the results show that the instability phenomena are based on the density change or high density itself. Therefore, the analysis for air condition with high density & pressure and atmospheric condition were also evaluated for comparison. For the evaluation, the RHS of the equation is separated as in (3).

$$\frac{\partial}{\partial X} \left( \frac{\rho h^3}{k_x \mu} \frac{\partial p}{\partial X} \right) = \left( \frac{hu}{2} \right) \frac{\partial \rho}{\partial X} + \left( \frac{u}{2} \frac{\partial h}{\partial X} \right) \rho + \frac{\partial(\rho h)}{\partial t} \quad (3)$$

The first term of the RHS around the shaft is plotted in Fig. 8 and the second term is shown in Fig. 9. From these figures, it is concluded that the significant difference between the high density air and the S-CO<sub>2</sub> condition is caused by the first term of RHS in eq. (3). Total values of the RHS around the shaft is plotted in Fig. 10. The specific pressure distribution is shown in Fig. 11. The forces calculated from this distribution is organized as Table III. From Table III, it is concluded that the density changes induce  $F_x$  to become larger. This also explains the tendencies from Fig. 8

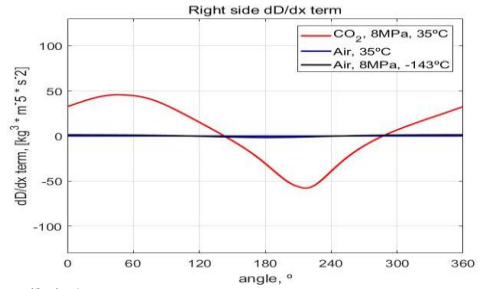


Fig. 8.  $\left( \frac{hu}{2} \right) \frac{\partial \rho}{\partial X}$  around the shaft,  $\epsilon = 0.25$  and 30,000 RPM

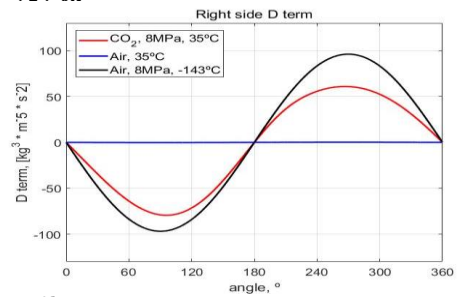


Fig. 9.  $\left( \frac{u}{2} \frac{\partial h}{\partial X} \right) \rho$  around the shaft,  $\epsilon = 0.25$  and 30,000 RPM

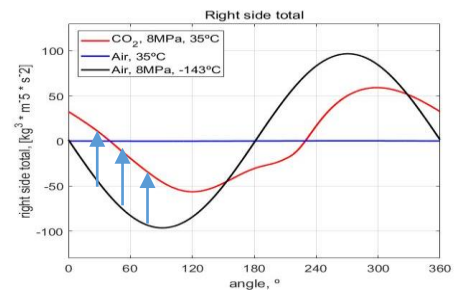


Fig. 10 . RHS total around the shaft,  $\epsilon = 0.25$  and 30,000 RPM

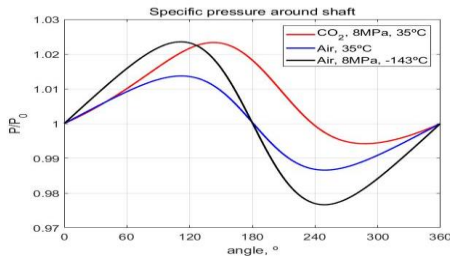


Fig. 11. Pressure distribution around the shaft,  $\epsilon = 0.25$  and 30,000 RPM

Table III. Force on the shaft,  $\epsilon = 0.25$  and 30,000 RPM

Thermal condition	$F_x$ (N)	$F_z$ (N)
Air at 0.1 MPa, 35 °C	0.021	-1.852
Air at 8 MPa, -143 °C	0.854	-256.4
CO <sub>2</sub> at 8 MPa, 35 °C	100.8	-124.5

## 2.2 Experimental analysis of magnetic bearing instability

During the experiment, the CO<sub>2</sub>'s thermal state is controlled by S-CO<sub>2</sub> pressurizing experiment (S-CO<sub>2</sub>PE) facility. The AMB test rig is attached to this facility as shown in Fig. 12. The AMB test rig consists of the compressor and the AMB. The impeller is removed so only the bearing effect is expected to be dominant.

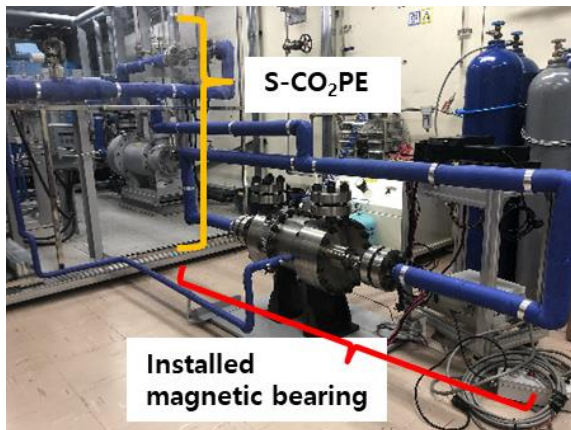


Fig. 12. The AMB & compressor system for S-CO<sub>2</sub>

The tests are proceeded for different RPM under 9 MPa & 50 °C (350kg/m<sup>3</sup>) conditions. The shaft trajectory is shown in Fig. 13. It is observed that the shaft motion does not keep single revolving center when the RPM increases.

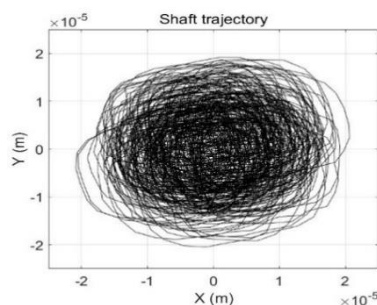


Fig. 13. Shaft trajectory data from S-CO<sub>2</sub> test and 30,000 RPM

As substituting this position data into the lubrication model, the lubrication force,  $F_{LUB}$  is obtained. This is fitted with the eccentricity ratio in Fig. 14.

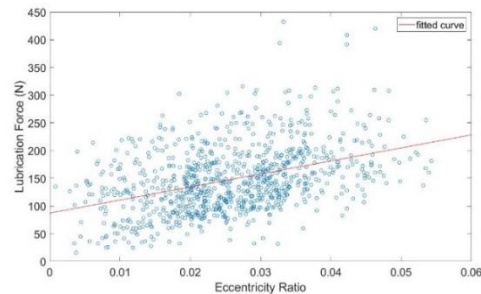


Fig. 14.  $F_{LUB}$  with 30,000 RPM ( $K_x Re^{n_x}$  : Turbulence intensity)

From this relationship, the stiffness is 6.47 N/ $\mu$ m but it seems that  $F_{LUB}$  has weak relationship with eccentricity ratio. To explain this, the transient motion and the density change are expected to be the reason. The method to quantify the transient effect is planned for additional fitting.

To analyze the effect of  $F_{LUB}$  with non-uniform stiffness and damping coefficient, the operation with vacuum condition and S-CO<sub>2</sub> condition is compared after Fast Fourier Transform (FFT) was applied. The results of FFT with 5 operation speeds are plotted as waterfall plot in Fig. 15 for S-CO<sub>2</sub> condition.

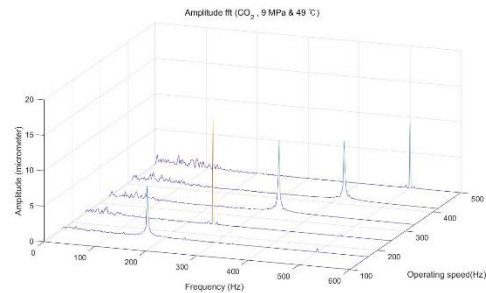


Fig. 15. FFT of the shaft trajectory data from S-CO<sub>2</sub> test

The low frequency range is main region of the lubrication instability effect. There is significant noise but no clear peak for lubrication whirl or whip. It seems that the operation speed is not high enough in comparison with critical speed.

To analyze the lubrication instability effect, the test with higher speed near critical speed is planned. In addition, comparison with FFT of vacuum condition will be proceeding.

## 3. Conclusions

From the developed lubrication model, it is concluded that the instability of the magnetic bearing control can be caused by S-CO<sub>2</sub>'s physical properties. Based on this results, a magnetic bearing experimental facility is constructed. Tests for various RPMs were performed for verifying the model and the instability sources. The comparison between the model and the tests shows that the transient change of the shaft motion and the fluid physical properties could cause the instability. Also, the

complex geometry and heating effect can amplify the transient change. To analyze this, the near-critical speed test with gap-filled magnetic bearing is planned to commence in the near future. From this test, it is expected that the lubrication effects like whirl or whip with close to ideal geometry can be finally compared.

Furthermore, the magnetic bearing's stiffness and damping coefficient will be analyzed for transient model. With this, dynamics of the shaft can be established for several different conditions. Well validated model can be adapted to MMR with transient operation. After developing an accurate model, the control logic of the magnetic bearing can be finally suggested.

#### **Acknowledgement**

This research was supported by Civil-Military Technology Cooperation Program (ICMTC) funded by the Agency for Defense Development (17-CM-En-04).

#### **REFERENCES**

- [1] Kim, S. G., Yu, H., Moon, J., Baik, S., Kim, Y., Jeong, Y. H., and Lee, J. I. (2017) A concept design of supercritical CO<sub>2</sub> cooled SMR operating at isolated microgrid region. *Int. J. Energy Res.*, 41: 512–525. doi: 10.1002/er.3633.
- [2] Tsuji, Tomoya, et al. "Solubility and Liquid Density Measurement for CO<sub>2</sub>+ Lubricant at High Pressures." Asian Pacific Confederation of Chemical Engineering congress program and abstracts Asian Pacific Confederation of Chemical Engineers congress program and abstracts. The Society of Chemical Engineers, Japan, 2004.
- [3] Seeton, Christopher J., and Predrag Hrnjak. "Thermophysical properties of CO<sub>2</sub>-lubricant mixtures and their affect on 2-phase flow in small channels (less than 1mm)." (2006).
- [4] Sienicki, James J., et al. "Scale dependencies of supercritical carbon dioxide Brayton cycle technologies and the optimal size for a next-step supercritical CO<sub>2</sub> cycle demonstration." *SCO<sub>2</sub> power cycle symposium*. 2011.
- [5] Shelke, Santosh. "Controllability of Radial Magnetic Bearing." *Procedia Technology* 23 (2016): 106-113.
- [6] Hamrock, Bernard J., Steven R. Schmid, and Bo O. Jacobson. *Fundamentals of fluid film lubrication*. CRC press, 2004.
- [7] Taylor, C. M., and D. Dowson. "Turbulent lubrication theory—application to design." *Journal of Lubrication Technology* 96.1 (1974): 36-46.